Marine Geology 462 (2023) 107079

Contents lists available at ScienceDirect

Marine Geology

journal homepage: www.elsevier.com/locate/margo

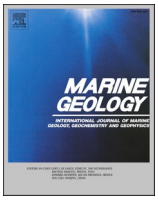

Cohesion, permeability, and slope failure dynamics: Implications for failure morphology and tsunamigenesis from benchtop flume experiments

Maxwell M.W. Silver [a,*], Brandon Dugan [a,b]

[a] Hydrologic Science and Engineering Program, Colorado School of Mines, Golden, CO, USA
[b] Department of Geophysics, Colorado School of Mines, Golden, CO, USA

ARTICLE INFO

Editor: Michele Rebesco

Keywords:
Physical experiments
Submarine slope failure
Overpressure
Excess head
Cohesion
Permeability
Factor of safety

ABSTRACT

Submarine slope failures pose hazards to coastal communities through their ability to damage seafloor infrastructure and generate tsunamis. Submarine slope failures occur along continental margins worldwide, yet our understanding of submarine slope failure evolution and tsunamigenic potential is limited. Overpressure has been a proposed mechanism for initiating and preconditioning for slope failures, but understanding of its role in slope failures is limited. In this study, we investigate overpressure-induced slope failures with different sediment compositions and properties common in the marine environment. Overpressure required for slope failure and failure behavior were investigated in relation to sediment permeability and cohesion. We investigated failures in benchtop flume experiments using mixtures of fine-grained quartz sand and cohesive smectite clay or fine-grained quartz sand and non-cohesive clay-sized quartz. In high-permeability, sand-rich systems (0–5 wt% smectite), overpressure required to induce failure directly related to smectite content (R^2 of 0.89). At smectite concentrations of 25 wt% or greater, normalized overpressure (λ^*) required to induce slope failure remained constant at $\lambda^* = 1.52 \pm 0.55$. Failure behavior also changed at 25% smectite. In sand-rich systems, a single failure event occurred even with sustained or increased overpressure. With smectite or clay-sized quartz concentrations of 25 wt% or higher, a series of slope failures occurred. Concentrations of smectite $\geq$25% also produced larger and more brittle failure deformation features (e.g., tension cracks and subsurface fissures). We conclude that lower permeability systems have the potential for larger failures and cohesive sediment mixtures are necessary for producing brittle failure features (e.g., tension cracks, subsurface fissures, rafted blocks, etc.). Experiments using 25, 75, and 90 wt% smectite produced rafted sediment blocks separated from the parent slope. However, experiments did not mobilize any intact blocks downslope even with a relatively steep (19°) slope. Observed experiment failure deformation features (e.g., mud-volcanism, tension cracks, clay-enriched toe deposits, etc.) match observed phenomenon in natural marine environments. From our experiments, we interpret in the presence of low-permeability, high-cohesion sediments, overpressure can produce non-tsunamigenic submarine slope failures and precondition slopes for tsunamigenic failure. Thus, our work demonstrates the importance of sediment properties and composition in relation to the types of failures produced and additionally emphasize the need for multiple factors (e.g., excess head plus seismic shaking) to mobilize large, rafted blocks downslope which has direct impact in improving coastal hazard assessment.

1. Introduction

Submarine slope failures pose hazards to coastal communities through their ability to damage seafloor infrastructure and generate tsunamis (Tappin et al., 2001; Kvalstad et al., 2005; Fine et al., 2005). The resulting tsunamis can result in many lost lives (e.g., > 2000 lives lost in Papua New Guinea; Tappin et al., 2001) and damage to coastal infrastructure (e.g., nuclear power plants, fisheries, harbors, and utilities; Tappin et al., 2008, 2014; Tewfik et al., 2008; Garces et al., 2010; ten Brink et al., 2014; Williams et al., 2022). Submarine slope failures have occurred in active and passive continental margins (Bondevik et al., 2005; Tappin et al., 2008; Locat et al., 2009; Harbitz et al., 2014; Scholz et al., 2016) and on low angle marine slopes (< 2°; Prior et al., 1986; Watts, 1997; Urlaub et al., 2012), yet understanding of submarine slope failure initiation, evolution, and tsunamigenic potential is limited and sometimes a contentious topic (Bondevik et al., 2005;

* Corresponding author.
E-mail address: mmsilver@mines.edu (M.M.W. Silver).

https://doi.org/10.1016/j.margeo.2023.107079
Received 29 November 2022; Received in revised form 22 May 2023; Accepted 27 May 2023
Available online 9 June 2023

Tappin et al., 2008; Vanneste et al., 2011).

Sediment properties and geological environment play vital roles in submarine slope stability and failure evolution. Pore pressure and seismic accelerations are often proposed as slope failure initiators (Lemke, 1967; Prior et al., 1982; Hampton et al., 1996; Stigall and Dugan, 2010). Other factors, such as shear strength and depositional history are classified as slope failure preconditioning factors. Preconditioning factors also affect the mobility and evolution of failed sediments (e.g., hydroplaning, slumping, and fluidization), nature of failure (e.g., retrogressive), and post-failure morphology (e.g., turbidites, debris flow deposit, blocks; Terzaghi, 1956; Mohrig et al., 1999; Elverhøi et al., 2000, 2002; Mohrig and Marr, 2003; Silver and Dugan, 2020; Kaminski et al., 2020).

We advance the state of knowledge of submarine slope failures by characterizing how permeability and cohesion impact pressure required to trigger a slope failure the evolution and morphology of submarine slope failures. This is a critical step for improving our understanding of submarine-landslide-induced tsunamis. We accomplish this via a suite of benchtop flume physical experiments with sediment compositions and a geometry representative of a prograding submarine river delta on a passive margin. Although our experiments do not represent a direct scaling of natural systems, they provide direct test of sediment conditions (e.g., cohesion, overpressure, permeability) and failure type and size.

2. Background

Submarine slope failures occur less frequently on passive margins than on seismically active margins (Mosher, 2009; ten Brink et al., 2016), but passive margins are still vulnerable to submarine slope failures. In 1929 a magnitude (M_L) 7.2 earthquake triggered the Grand Banks slide offshore Newfoundland, Canada (Fine et al., 2005; Schulten et al., 2019). The slide mobilized 200 km^3 of sediment at speeds of 15–30 m/s for distances up to 1000 km, severed transatlantic communication cables, and produced a tsunami that killed 28 people (Fine et al., 2005; Løvholt et al., 2019). Other studies of the US Atlantic margin found the region to be vulnerable to submarine landslide-generated tsunamis, particularly due to the densely populated coastline, port facilities, industrial sites, and coastal nuclear power plants (ten Brink et al., 2009, 2014).

Experimental, modelling, and geological studies of submarine slope failures along passive margins has revealed the importance – or even necessity – of overpressure in submarine slope deformation and failure (Hampton et al., 1996; Dugan and Flemings, 2000; Bondevik et al., 2005; Solheim et al., 2005; Strout and Tjelta, 2005; Gue et al., 2010; Elverhoi et al., 2010; Elverhøi et al., 2010; Gamboa et al., 2011; Dugan and Sheahan, 2012; Liu et al., 2019; Kawakita et al., 2020). Seismic accelerations have also been suggested to be a requirement for slope failure initiation (Ohmachi, 2003; McAdoo et al., 2004; Biscontin et al., 2004; Biscontin and Pestana, 2006; Gee et al., 2006; Strasser et al., 2007; Masson et al., 2011; ten Brink et al., 2016). However, seismic accelerations may increase the strength of sediments and reduce failure size (Mosher, 2009; Sawyer and DeVore, 2015; ten Brink et al., 2016). Sawyer and DeVore (2015) suggest that low-energy seismic accelerations along active margins trigger frequent, small-scale slope failures which prevents thick sediment accumulations that are a key contributor to large, tsunamigenic failures. Slope failure recurrence interval on passive margins has been shown to be longer than on active margins (Mosher, 2009), facilitating accumulation of thicker sediment sequence which can create larger failures (compared to active margins) (ten Brink et al., 2016).

Despite the risks posed by submarine landslide-induced tsunamis, little is known about how initial in-situ conditions of a submarine slope influence development during failure, which directly relates to tsunamigenic potential. Some studies have characterized slope failure deposits, including their lithology, structure, seismic attributes, geometry, and morphology (Prior et al., 1986; McAdoo et al., 2000; Gazioğlu et al., 2005; Locat et al., 2010; Scholz et al., 2016; Clare et al., 2019). Other studies have modelled submarine landslide tsunamigenesis, typically making assumptions about slide evolution (e.g., slump/block behavior, velocity; (Harbitz et al., 1993; Bardet et al., 2003; Finn, 2003; Lynett and Liu, 2003; Ohmachi, 2003; Hornbach et al., 2007; Zengaffinen et al., 2020) which are affected by in-situ slope conditions.

3. Methods

We investigated submarine slope failure in a 2D marine delta-like environment using a benchtop flume in the Colorado School of Mines Geomechanics Laboratory (Fig. 1; Silver and Dugan, 2020). We created a system with a low-permeability layer overlying a higher-permeability layer, a stratigraphic pattern present in many marine deltas (e.g., Elverhøi et al., 2010) and channel-levee deposits (e.g., Stigall and Dugan, 2010). The higher permeability layer allowed us to control overpressure in a slope failure system influenced by flow focusing (e.g., Osborne and Swarbrick, 1997; Dugan and Flemings, 2000; Stigall and Dugan, 2010). The high and low permeability layers were separated by a fine mesh to prevent mixing of sediments. Sediment compositions of the overlying lower-permeability layer were modified to investigate the role of cohesion and permeability in overpressure-induced slope failures.

We induced slope failures in the lower-permeability layer via incremental increases in overpressure in fully saturated, submerged sand-clay mixtures. In our experiments, we controlled overpressure by inducing excess head (hydraulic head above hydrostatic conditions) in 1–1.5 cm increments. The lower-permeability layer was composed of mixtures of commercially obtained fine-grained quartz sand (sand-sized grains; sub-angular quartz; 87% SiO_2; D_{50} = 195 μm; 2.65 g/cm^3) and dioctahedral smectite (bentonite) clay (63% SiO_2 and 21% Al_2O_3; D_{90} = 44 μm; 2.6 g/cm^3) or non-cohesive, clay-sized quartz (silica powder; 99.8% SiO_2; D_{90} = 137.2 μm; 2.65 g/cm^3). Smectite was selected for its cohesive properties (Odom, 1984) and prevalence in natural shelf-slope systems (Underwood and Deng, 1997; Steurer and Underwood, 2003; Forsberg and Locat, 2005). Clay-sized quartz was selected to replicate the grainsize of smectite while isolating the effects of cohesion. Sediment mixtures were constrained to a constant pre-failure slope geometry measuring 30.3 cm long, 9.8 cm deep, and 6.8 cm tall, with a top horizontal surface 10.7 cm in length that tapered to the base of the flume (Fig. 1). The tapered slope was 19.4°, which is below the angle of repose for all sediment mixtures (Beakawi Al-Hashemi and Baghabra Al-Amoudi, 2018). This slope angle provided a representation of a relatively steep slope, relative to a natural marine system where slopes are generally <4°, without driving failure due to oversteepening, thus allowing sediment remobilization due to overpressure.

We studied slope failure in mixtures (wt%) of: (1) 25% smectite and 75% fine-grained (FG) quartz sand; (2) 50% smectite +50% FG sand; (3) 75% smectite +25% FG sand; (4) 75% clay-sized quartz +25% FG sand; (5) 90% smectite clay +10% FG sand; and (6) 100% smectite. Sediment mixtures were homogenized in a counter-top mechanical mixer for 20 min with 15 wt% water and 85 wt% sediment. Homogenized mixtures were poured into the flume and shaped with a template to create a consistent slope geometry. The flume was then filled with tap water over an effluent weir until the flume water height reached the height of the effluent weir (Fig. 1). Then Reservoir 2 (R2) was filled (Fig. 1) to a water level matching the flume water height. The system was left undisturbed for a minimum of 24 h to facilitate saturation and equilibration to hydrostatic conditions. During this 24-h saturation period, water was supplied adjacent to the effluent weir at low flow to compensate for evaporative losses.

Experiments were performed by raising the water level in R2 in 1 or 1.5 cm increments to increase overpressure at the boundary between the high-permeability and low-permeability layers. Five-minute pauses were taken after each raising of head in R2. When slope failure occurred, the time of the event, nature of failure, and overpressure ($r_w gh^*$; rw =

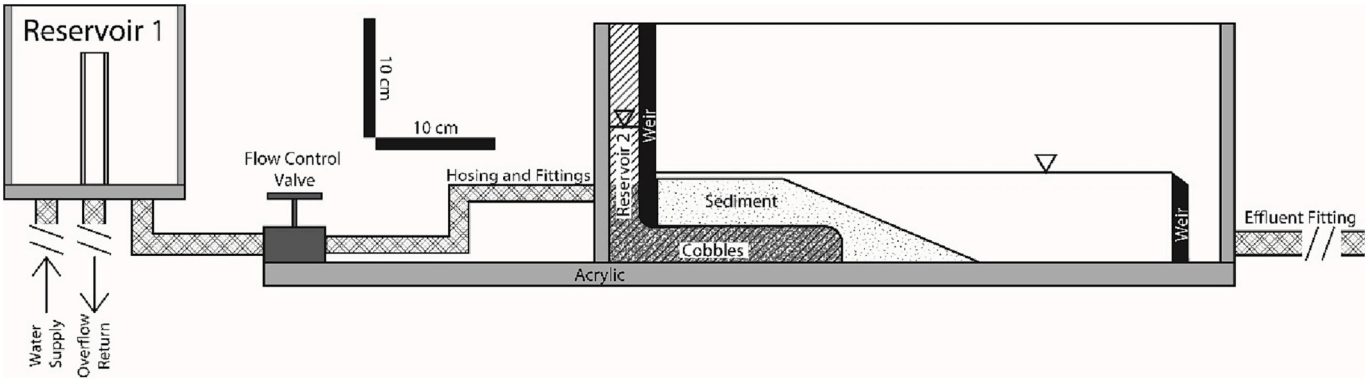

Fig. 1. Schematic diagram of the benchtop flume in the Geomechanics Laboratory at the Colorado School of Mines. The area labelled "sediment" represents the typical experiment slope geometry (e.g., the lower-permeability layer). R2 is denoted with diagonal (45°) hatching. Replicated from Silver and Dugan (2020).

water density, g = acceleration due to gravity, h* = head above hydrostatic) before and after the event were recorded. Slope failure was defined as any visible slope deformation during the experiment. Failure deformation features (i.e., tension cracks, boils, eruptions, etc.) were characterized for all sediment mixtures. Experiments were ended once overpressure in R2 stabilized and no longer responded to further attempts to increase R2 water height (i.e., permeability of the slope was high enough that overpressure subjected on the slope could no longer be increased). For each mixture, experiments were repeated until three successful runs were observed, where success was defined as: (1) slope failure not occurring during setup (e.g., not during sediment submergence and saturation) and (2) the entirety of slope failure being captured via videography. Videography and photogrammetry were used to help interpret failure behavior.

Observed overpressure required to induce slope failure was mapped to normalized overpressure (λ^*) in terms of effective vertical stress assuming hydrostatic conditions (σ'_{vh}; Bekins et al., 1995):

$$\lambda^* = \frac{\rho_w g h^*}{\sigma'_{vh}} \tag{1}$$

$$\sigma'_{vh} = (\rho_b - \rho_w)\mathrm{g}z \tag{2}$$

where z is depth from the water-sediment interface to the low permeability-high permeability interface (3.5 cm), and ρ_b is bulk density. Bulk density was measured in triplicate and averaged for each experiment sediment mixture. Normalized overpressure provided dimensionless scaling of overpressure, allowing scaling from flume conditions to geological-scale systems.

4. Results

Normalized overpressure required to induce failures in our slope systems revealed two distinct failure regimes, the first in sand-rich mixtures (clay grainsize content ≤5 wt%; Fig. 2) and the second in intermediate to clay-rich mixtures (clay grainsize content ≥25 wt%; Fig. 3). Our previous physical experiments (Silver and Dugan, 2020) of fine-grained, sand-dominated systems found normalized overpressure (λ^*) required to induce slope failure increased linearly with smectite clay content (cc_{sm}; $R^2 = 0.91$):

$$\lambda^* = 0.15cc_{sm} + 0.38 \tag{3}$$

with λ^* ranging from an average of $\lambda^* = 0.32 \pm 0.04$ ($h^* = 1.30 \pm 0.14$ cm) at 0 wt% smectite clay to $\lambda^* = 1.10 \pm 0.08$ ($h^* = 4.43 \pm 0.33$ cm) at 5 wt% smectite clay (Table 1 **and** Fig. 2; Silver and Dugan, 2020). In this fine-grained, sand-rich regime, slope failure occurred as a singular event (i.e., surface eruption or subsurface fissure evolving into a surface blow-out). This failure event created a flow conduit that increased system permeability to a level sufficient to relieve any additional increases in overpressure. As such, additional failures were not induced.

In systems with intermediate concentrations of clay-sized particles (25–50 wt% smectite; 75 wt% clay-sized quartz) and smectite-rich

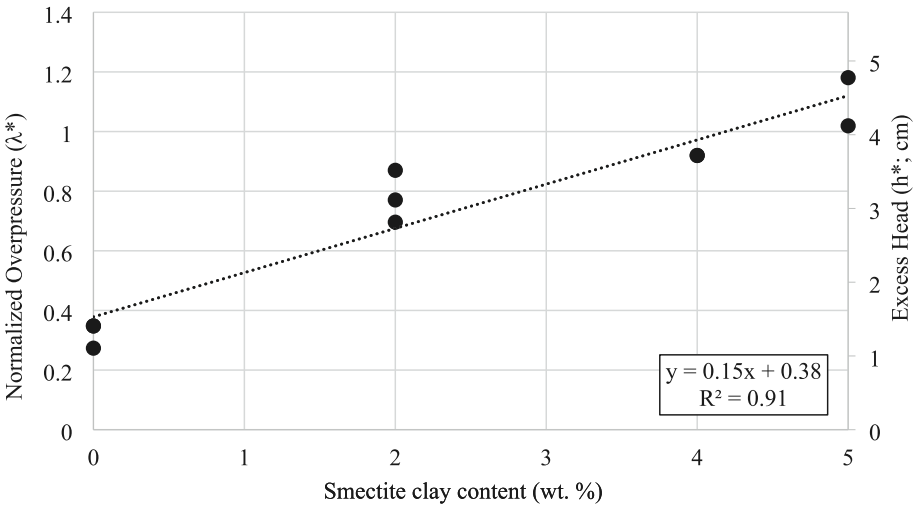

Fig. 2. Normalized overpressure (λ*) and excess head (cm) required to induce slope failure as a function of smectite clay content (wt%) mixed with fine-grained (FG) quartz sand. Each data point represents an individual experiment.

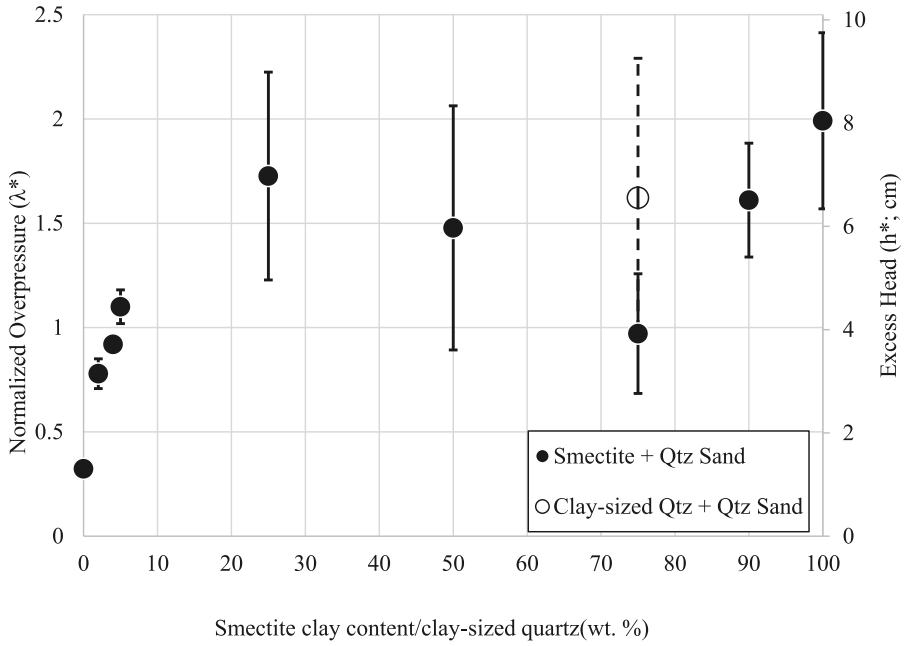

Fig. 3. Averages of normalized overpressure (λ*) and excess head (h*) required to induce slope failure as a function of smectite clay content (wt%) or clay-sized quartz (qtz) mixed with fine-grained (FG) qtz sand (grainsize). Error bars are one standard deviation. Open circle and dashed error bars are for the clay-sized qtz + qtz sand data.

Table 1
Average normalized overpressure (λ^*) and excess head (h^*) required for slope failure as a function of clay content (smectite or clay-sized quartz). Sediment compositions were mixtures of clay and fine-grained quartz sand.

Sediment Composition (wt%)	Average Normalized Overpressure at Failure (λ*)	Average Excess Head at Failure (cm)
100% FG Qtz Sand (no clay)	0.32 ± 0.04	1.30 ± 0.14
2% Smectite	0.78 ± 0.07	3.13 ± 0.29
4% Smectite	0.92 ± 0.00	3.70 ± 0.00
5% Smectite	1.10 ± 0.08	4.43 ± 0.33
25% Smectite	1.73 ± 0.50	6.95 ± 2.00
50% Smectite	1.48 ± 0.59	5.95 ± 2.35
75% Smectite	0.97 ± 0.29	3.91 ± 1.15
75% Clay-Sized Qtz	1.62 ± 0.67	6.53 ± 2.69
90% Smectite	1.61 ± 0.27	6.48 ± 1.10
100% Smectite (no sand)	1.99 ± 0.42	8.01 ± 1.70

concentrations (90–100 wt% smectite), there was no statistically significant correlation (R^2 of 0.0008) between normalized overpressure required to induce slope failure and clay grainsize content. In experiments using ≥25 wt% smectite or clay-sized quartz, normalized overpressure required to induce failure remained relatively constant ($\lambda^* = 1.52 \pm 0.55$; $h^* = 6.12 \pm 2.22$ cm; Fig. 3). Normalized overpressure required to induce slope failures averaged $\lambda^* = 1.73 \pm 0.50$ ($h^* = 6.95 \pm 2.00$ cm) at 25 wt% smectite, $\lambda^* = 1.48 \pm 0.59$ ($h^* = 5.95 \pm 2.35$ cm) at 50 wt% smectite, $\lambda^* = 1.62 \pm 0.67$ ($h^* = 6.53 \pm 2.69$ cm) at 75 wt% clay-sized quartz, $\lambda^* = 1.61 \pm 0.27$ ($h^* = 6.48 \pm 1.10$ cm) at 90 wt% smectite, and $\lambda^* = 1.99 \pm 0.42$ ($h^* = 8.01 \pm 1.70$ cm) at 100 wt% smectite (Table 1 **and** Fig. 3). Normalized overpressure required to induce slope failure in 75 wt% smectite concentrations was lower than these other systems, with $\lambda^* = 0.97 \pm 0.29$ ($h^* = 3.91 \pm 1.15$ cm; Table 1).

Normalized overpressures required to induce slope failures in benchtop flume experiments were compared to an infinite slope Factor of Safety (FS) approximation of slope stability (**Eq. 4**; Terzaghi et al., 1996):

$$FS = \frac{c + \left(\sigma'_{vh}\cos^2\theta - \rho g h^*\right)\tan\phi_f}{\sigma'_{vh}\cos\theta\sin\theta} \quad (4)$$

where c is cohesion, σ'_{vh} is vertical effective stress assuming hydrostatic conditions, θ is seafloor slope, and ϕ_f is internal friction angle. This equation relates slope stabilizing and slope destabilizing forces, and $FS < 1$ indicates slope failure, We used **eq. 4** to predict the critical excess head (h^*) needed to induce slope failure at $FS = 1$ and present the results as normalized overpressure (**eq. 1**), assuming c increases at 10 Pa per 1 wt% smectite (Silver and Dugan, 2020), internal friction angle was 35° for 100% fine-grained sand and decreased by 0.1° per each wt% clay added (Silver and Dugan, 2020). For all calculations θ was 19° (the same as our experiments), σ'_{vh} was calculated for 3.5 cm depth below the water-sediment interface (a commonly observed failure initiation depth in experiments), and bulk density was 1800 kg/m^3. **Eq. 4** predicts λ^* well for smectite concentrations ≤25 wt% ($R^2 = 0.91$), but overpredicts λ^* at higher smectite concentrations and for 75 wt% clay-sized quartz ($R^2 = 0.54$) (Fig. 4). The FS analysis predicts a linear increase in normalized overpressure (λ^*) required to induce slope failure with clay content. However, the observed constant normalized overpressure at failure with clay concentrations ≥25 wt%, including cohesive and non-cohesive clays, is inconsistent with the infinite slope approximation's predictions (Fig. 4).

4.1. Failure evolution with clay content

Smectite clay content also affected failure behavior and evolution. In 0 wt% smectite experiments (100 wt% FG sand), a singular failure event was observed; once overpressure required to induce failure was reached and failure occurred, additional increases in overpressure did not produce additional failure events. Subsequent increases in overpressure did not produce additional failures because surface eruptions created flow pathways which increased system permeability. Flow was focused through these high permeability pathways in the overburden which prevented failure elsewhere.

In experiments using sediment mixtures with ≥25 wt% smectite (including 75 wt% clay-sized quartz), multiple failure events were

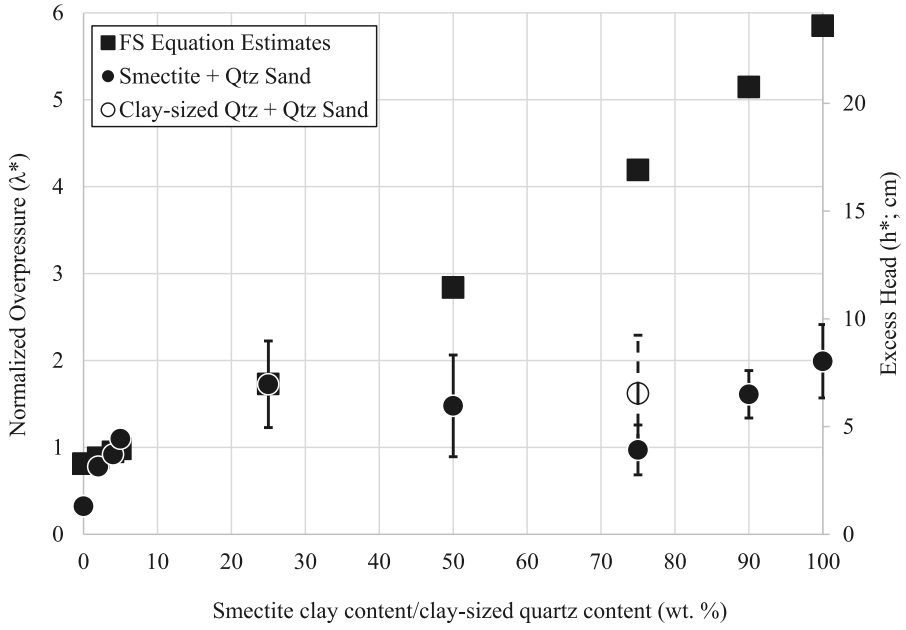

Fig. 4. Normalized overpressure (λ*) and excess head (h*) required to induce slope failure and λ* predicted by the Factor of Safety (FS) equation (**Eq.** 4) as a function of smectite or clay-sized quartz (qtz). For λ* predicted, c was assumed to increase at 10 Pa per 1 wt % smectite, θ was set to 19° (the same as experiments), σ'_{vh} was calculated for 3.5 cm, and ρ was assumed to be 1800 kg/m^3. Error bars are one standard deviation. Open circle and dashed error bars are for the clay-sized qtz + qtz sand data.

observed when overpressure was maintained (Fig. 5). With additional increases in overpressure, failure occurred at different overpressure values. In experiments with 25, 90, and 100 wt% smectite, the overpressure required to induce additional failure after the initial failure event increased with successive failure events (see **supplemental material**). In experiments with 50 and 75 wt% smectite or 75 wt% clay-sized quartz, overpressure required to induce additional failure events did not show a consistent trend (see **supplemental material**).

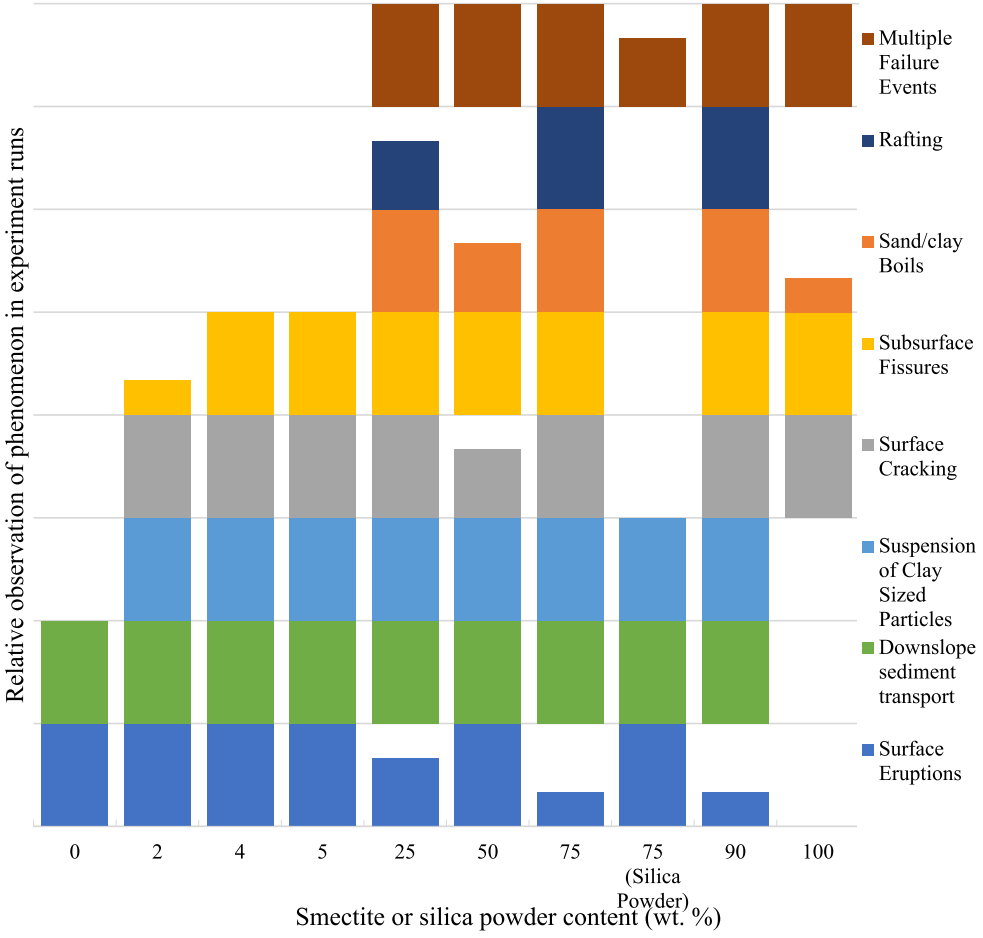

Fig. 5. Failure behaviors observed in experiments. Heights of bar sections are based on the percentage of experiment runs in which behavior was observed. Surface eruptions and downslope sediment transport were observed in all mixtures except those using 100 wt% smectite. Suspension of smectite or silica powder particles in the water column was observed in all mixtures containing both FG sand and smectite or clay-sized quartz. Surface cracking and subsurface fissure formation was observed in all mixtures containing smectite clay. Sand/clay boil formation was observed in mixtures containing smectite clay at ≥25 wt %. Rafting of sediment blocks was observed in FG sand + smectite mixtures of 25, 75, and 90 wt%. Multiple failure events occurred in all mixtures containing ≥25 wt% smectite or clay-sized quartz.

Experiments performed without smectite (e.g., 0 wt% smectite and 75 wt% clay-sized quartz) were cohesionless and produced surface eruptions/sand volcanism and downslope grain flows (Table 2, Figs. 4 and 5). Similar to the 0 wt% smectite experiments, in systems with 2, 4, and 5 wt% smectite, surface eruptions/sand volcanism and downslope grain flows were observed (Table 2, Figs. 4 and 5). The addition of smectite, which increased cohesion, also resulted in brittle failure features (surface cracking/tension cracking and subsurface fissures) and suspension of smectite particles in the water column. As in 0 wt% smectite experiments, a singular failure event was observed in each experiment of 2–5 wt% smectite; once overpressure required to induce failure was reached and failure occurred, additional increases in overpressure did not produce additional failure events.

Slope failures in systems with smectite concentrations of 25, 75, and 90 wt% where similar to failures observed in 0–5 wt% smectite experiments (i.e., surface eruptions, downslope granular flows, tension cracking, subsurface fissures, and suspension of smectite particles). These experiments (25, 75, and 90% smectite), however, also produced sand/clay boils and separated (e.g., rafted) sediment blocks near the water-sediment interface (Table 2, Fig. 5). Unlike the systems with 0–5 wt% smectite, sequential failure events were observed in systems with 25–100 wt% smectite or 25 wt% FG Sand and 75 wt% clay-sized quartz. These sequential failure events were driven by additional increases in overpressure which was controlled in the experiments. In experiments with 25–100 wt% smectite, overpressure initially produced tension cracks and sand/clay boils. With additional increases in overpressure, subsurface fissures evolved into surface eruptions (blow-outs). In experiments with 25–100 wt% smectite, subsequent increases in overpressure also produced new subsurface fissures, rafted blocks, (excluding clay-sized quartz experiments), and surface blow-outs (Table 2 **and** Fig. 5).

Slope failures in systems with 50 wt% smectite contained the same slope failure features observed in systems with 2–5, 25, 75, and 90 wt% smectite. However, experiments with 50 wt% smectite did not produce rafted blocks. Systems with 50 wt% smectite had sequential slope failures like experiments with 25, 75, and 90 wt% smectite and experiments with 75 wt% clay-sized quartz, with the exception that overpressure required for sequential failures did not increase linearly (see **supplemental materials**).

Slope failures in 100 wt% smectite systems produced sand/clay boils and tension cracks. Downslope sediment transport, suspension of smectite particles, and surface eruptions were not observed. Pure smectite systems did have sequential slope failures like experiments with 25, 50, 75, and 90 wt% smectite (Table 2 **and** Fig. 5).

Experiments performed with 75 wt% non-cohesive clay-sized quartz and 25 wt% FG quartz sand produced similar failure features as observed in 0 wt% smectite experiments (e.g., surface eruptions and downslope sediment transport) with the addition of suspension of clay-sized quartz particles. No brittle deformation features (e.g., boils, cracking, fissures, or rafting) formed, which was different from what was observed in experiments with smectite. Unlike experiments with low concentrations of clay-sized particles (0–5 wt. wt% smectite), clay-sized quartz experiments produced multiple failure events like intermediate and smectite-rich experiments.

Surface eruptions and downslope sediment transport occurred in all experiments except those where the slope was 100 wt% smectite. Surface/tension cracking was observed in all experiments containing smectite. Subsurface fissures and the suspension of sediments in the water column occurred in all mixtures containing both sand and smectite (or clay-sized quartz in the case of sediment suspension). Rafting of sediment blocks occurred in systems with 25, 75, and 90 wt% smectite. Sequential failure events were observed in all sediment mixtures containing >5 wt% clay-sized grains.

5. Discussion

Based on our experimental results, we defined two different regimes for normalized overpressure and failure evolution which were influenced by smectite content: sand-rich (0–5 wt% smectite) versus intermediate to clay-rich environments (25–100 wt% smectite or 75% clay-sized quartz).

Sand-rich environments (0–5 wt% smectite) were characterized by a linear increase in normalized overpressure required to induce slope failure with clay. We interpret the direct relationship between clay content and normalized overpressure at failure for systems with low smectite concentrations was a result of a reduction in system permeability as clay particles filled pore spaces between sand grains. As system permeability decreased, the rate at which overpressure could be dissipated decreased, resulting in higher pressure in the system. Overpressure would build, ultimately building to pore pressures sufficient to induce slope failure.

When comparing precited and observed normalized overpressures (λ^*) at failure, **Eq. 4** predicts λ^* well for smectite concentrations ≤25 wt % ($R^2 = 0.91$), but overpredicts λ^* at higher smectite concentrations and for 75 wt% clay-sized quartz ($R^2 = 0.54$). This indicates that factors other than cohesion and permeability are influencing λ^* at higher clay concentrations. Furthermore, λ^* predictions and observations exceeded 1.0 in several sand-clay systems (Table 1, Figs. 2 - 4). We attribute λ^* values >1.0 to the fact that cohesion (~10 Pa per 1% smectite), overpressure (~98 Pa per 1 cm h^*), and effective vertical stress (~550 Pa at $z = 3.5$ cm) are of similar magnitude in benchtop experiments. In natural systems where failures can be 10–100+ m thick, cohesion is the same as in the benchtop experiments (10s of Pa), however, overpressures and effective vertical stresses in natural systems are orders of magnitude higher (e.g., MPa; Osborne and Swarbrick, 1997b; Stigall and Dugan, 2010; Dugan and Sheahan, 2012).

Table 2
Slope failure behavior and failure/deformation features as a function of clay content (smectite or clay-sized quartz). Failure behavior and features are presented in percentage of occurrence in experiments. Sediment compositions were mixtures of clay and fine-grained quartz sand.

Sediment Composition	Surface Eruptions	Sand/Clay Boils	Tension Cracks	Subsurface Fissures	Suspension of Clay Sized Particles	Downslope Sediment Transport	Rafting	Multiple Failure Events
100% FG Qtz Sand (no clay)	100%	0%	0%	0%	NA	100%	0%	0%
2% Smectite	100%	0%	100%	33%	100%	100%	0%	0%
4% Smectite	100%	0%	100%	100%	100%	100%	0%	0%
5% Smectite	100%	0%	100%	100%	100%	100%	0%	0%
25% Smectite	67%	100%	100%	100%	100%	100%	67%	100%
50% Smectite	100%	67%	67%	100%	100%	100%	0%	100%
75% Smectite	33%	100%	100%	100%	100%	100%	100%	100%
75% Clay-Sized Qtz	100%	0%	0%	0%	100%	100%	0%	67%
90% Smectite	33%	100%	100%	100%	100%	100%	100%	100%
100% Smectite (no sand)	0%	33%	100%	100%	0%	0%	0%	100%

We expand on this scaling by applying **eq. 4** to our experiment setup (z = 3.5 cm; **Eq. 2**) and a representative natural system (40 m thick failure) (Fig. 6). For comparison, we compare λ^* at failure (FS =1) for two scenarios: 1) our experiment setup: z = 3.5 cm, c = 10 Pa/1 wt% smectite, σ'_{vh} = 550 Pa, θ = 19°, ϕ_f = 35° at 100% *FG Sand* and decreased by 0.1° per each wt% clay added, and bulk density (ρ) = 1800 kg/m^3; and 2) a representative natural system: z = 40 m, c = 10 Pa/1 wt % smectite, σ'_{vh} = 706.32 KPa (z = 40 m), ϕ_f = 35° at 100% *FG Sand* and decreased by 0.1° per each wt% clay added, and ρ = 1800 kg/m^3. This comparison shows that in a natural system with $\sigma'_{vh,}$ multiple orders of magnitude larger than c and all other parameters matching experimental conditions, λ^* at failure is less than one at failure (Fig. 6).

We observed a reduction in normalized overpressure required to induce slope failure at 75 wt% smectite concentrations relative to other 25–100 wt% experiments. However, overpressure required to induce slope failure in 75 wt% clay-sized quartz experiments was consistent with other 25–100 wt% experiments. Based on the overall similar physical properties, we interpret the drop in overpressure required for failure in experiments with 75 wt% smectite was the result of a complicated interplay between sediment cohesion and grain distribution. Determining the exact cause of the drop in overpressure required for failure at 75 wt% smectite requires experiments and modelling beyond the scope of this study.

5.1. Failure evolution and clay content

Clay content also changed how deformation and failure evolved. In systems with 0–5 wt%, failure occurred as single events in the form of surface eruptions. These surface eruptions formed crater-like deposits (i.e., mud volcanoes, pockmarks, or craters (Løseth et al., 2009) similar to structures observed at the Storegga Slide (Solheim et al., 2005) and Lower Congo Basin (Andresen and Huuse, 2011), whose formation mechanisms are attributed to overpressure-generated fluid expulsion. The introduction of cohesive smectite (2–5 wt%) created minor brittle deformation features such as surficial tension cracking, surficial sand boils, and subsurface fissures, but failure always occurred as a surface eruption (Fig. 7). In these systems, once surface eruptions started, no additional failures occurred, despite additional increases in overpressure that we imparted on the system. In such instances, overpressure caused the formation of surface eruptions and preferential flow pathways, allowing dissipation of overpressure. This new preferential flow pathway prevented the buildup of sufficient overpressure to induce additional failures (Elger et al., 2018). This indicates that natural systems with 0–5 wt% clay are less likely to experience multiple failure events than systems with higher clay concentrations.

In systems with ≥25 wt% smectite or 75 wt% clay-sized quartz, multiple failure events occurred. These failure events increased system permeability through the formation of surface eruptions (clay-sized quartz experiments) or subsurface fissures that evolved into surface eruptions (smectite mixtures; blowout, subsurface to surface piping, hydraulic chimneys). Once the first slope failure event occurred, a preferential flow pathway was produced, system permeability was increased, overpressure was reduced, and failure stopped. However, this enhanced permeability was inadequate to prevent further buildup of overpressure. Thus, subsequent slope failures occurred when overpressure reached a new critical level. Compared to FG sand-rich systems and clay-sized quartz experiments, the increased cohesion of intermediate and smectite-rich mixtures resulted in the production of subsurface fissures and subsurface-to-surface piping when failure occurred. However, in instances where sequential failure events were observed, these preferential flow pathways were insufficient to prevent future buildup of overpressure. Once overpressure was raised past the newly established critical point, another failure event occurred, generating another preferential flow path, increasing system permeability, and establishing a new critical overpressure required for further failures (Mazzini et al., 2007; Manton et al., 2019).

In addition to the number of failure events, smectite content also altered failure behavior (Fig. 5). In systems with 100 wt% smectite, only surface cracks and clay boils were observed. We attribute the lack of downslope sediment transport, subsurface fissures, and surface eruptions in 100 wt% smectite systems to the strong (relative to the vertical stresses and overpressures in our experiments) and uniform cohesion (~1000 Pa) of the material.

In systems with 0–90 wt% smectite or 75 wt% clay-sized quartz, downslope sediment transport was observed. In experiments with ≥25 wt% smectite, smectite or clay-sized quartz particles were suspended in

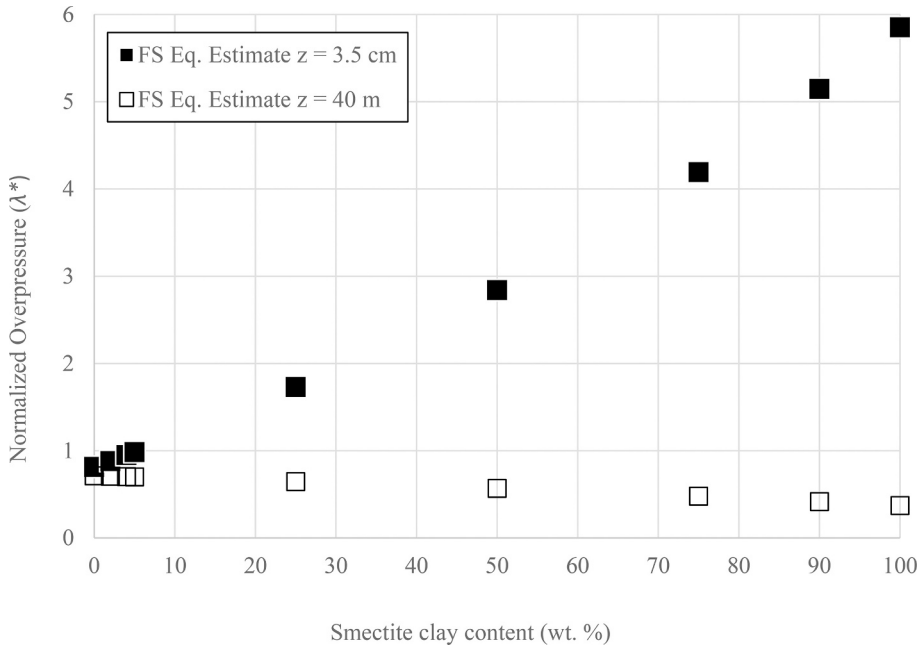

Fig. 6. Normalized overpressure (λ*) required to induce slope failure predicted by the Factor of Safety (FS) equation (**Eq. 4**) as a function of smectite or clay-sized quartz (qtz). c was assumed to increase at 10 Pa per 1 wt% smectite, θ was set to 19° (the same as experiments), σ'_{vh} was calculated for 3.5 cm (solid squares) or 40 m (hollow squares) depth below sea floor, and ρ was assumed to be 1800 kg/m^3.

the water column. These suspended particles were transported downslope and settled, forming smectite or clay-sized quartz-rich (relative to the rest of the slope) deposits near the slope's toe. This matches a mechanism proposed by (Elverhøi et al., 2010), who found clay-to-sand ratio as the key controlling parameter for the disparity between compact, disintegrating landslides and the formation of clay-rich distal deposits. Their physical experiments produced a distal, clay-rich deposit, matching our results and distal deposits observed at the Storegga Slide (Haflidason et al., 2004).

Surface cracking in smectite mixtures indicated dilation and localized strain with increased overpressure. The formation of these features in mixtures containing smectite reflects a necessity for cohesion in their formation. Without cohesive clay, pore pressure reduction formed as surface eruptions. Once cohesive clay particles were present, overpressure generated surficial cracking. However, flow rates alone were insufficient to completely reduce pressure back to hydrostatic conditions. Thus, to reduce overpressure, overall system permeability needed to increase. System permeability was increased through local formation of subsurface fissures.

Like surface cracking, the formation of subsurface fissures was dependent on the presence of cohesive clay. Subsurface fissures, however, only formed in mixtures containing sand and smectite. The absence of subsurface fissures in pure-sand mixtures and quartz sand + clay-sized quartz mixtures demonstrated the necessity for cohesive clays for surface cracks and subsurface fissure formation. The absence of subsurface fissures in quartz sand + clay-sized quartz mixtures also eliminated the possibility that grain-size distribution influenced the development of these features. The similar magnitude of excess head (~98 Pa per 1 cm h^*) to cohesive forces (10 Pa per 1 wt% smectite; Silver and Dugan, 2020) in our experiments can also be eliminated as a dominant factor in subsurface fissure formation, as subsurface fissures have been observed in nature where pore pressures can be orders of

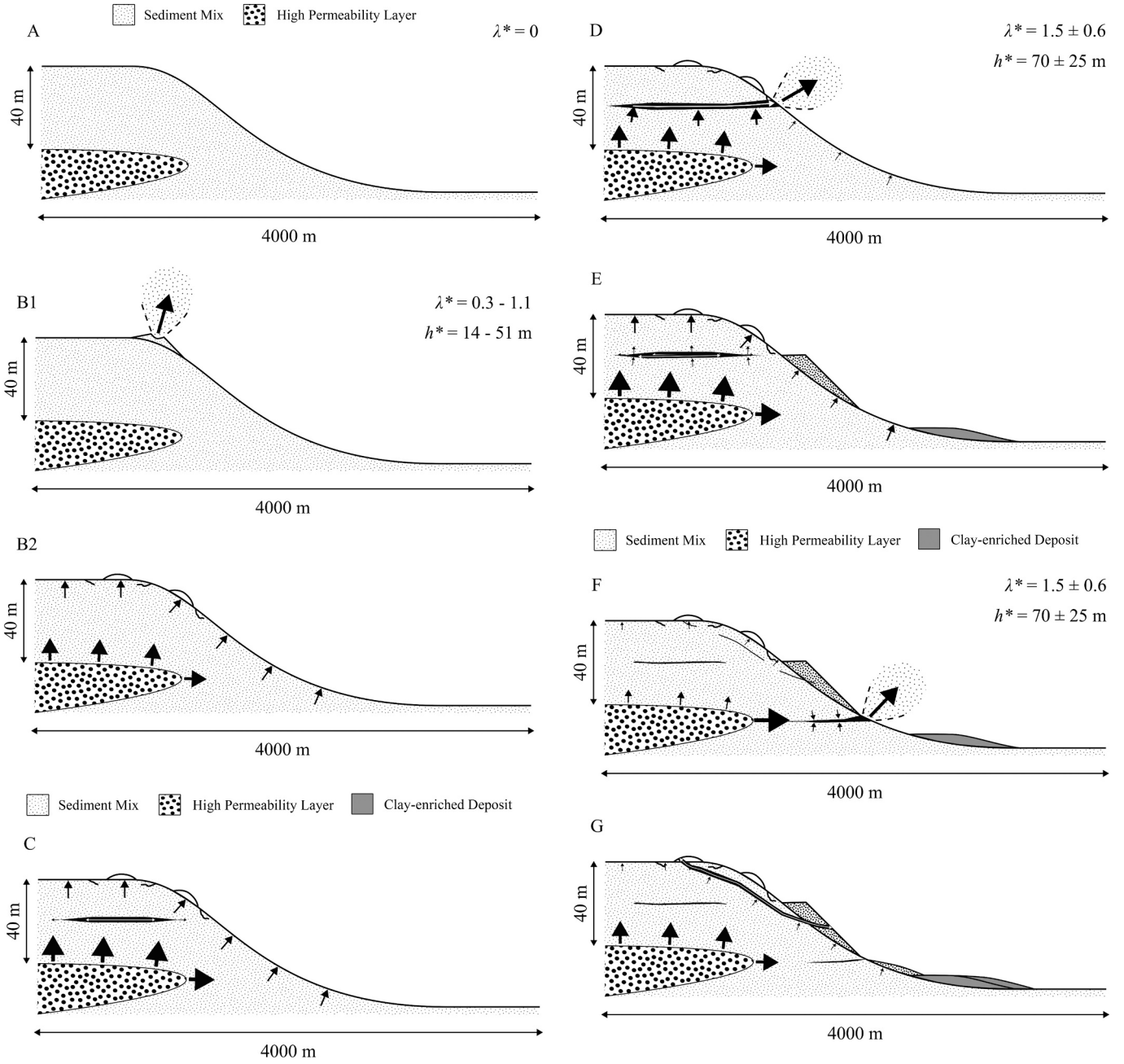

(caption on next page)

Fig. 7. Conceptual model scaling (geometrically) our flume experiments to geological-scale slope failure processes in an idealized marine delta cross section with hypothetical scenario scale bars. Arrow size and direction indicate pore fluid pressure (head) and flow direction, respectively. Normalized overpressure required to induce slope failure (λ^*) based on experiment observations is provided at moments of failure in the conceptual diagram and converted to absolute excess head (h^*) for the hypothetical scales shown using **Eq. 1**. Mixtures of 0 wt% smectite and 75 wt% silica powder only progressed from **A** to **B1**, with multiple iterations of step **B1** occurring in clay-sized quartz mixtures. Mixtures of 2–5 wt% smectite progressed from **A** – **F**, skipping **B1**. Smectite mixtures ≥25 wt% progressed from **A** – **G**, skipping **B1**. **A.** A simplified marine shelf slope under hydrostatic conditions ($\lambda^* = 0$). **B1.** Non-cohesive sediment mixtures. Overpressure builds and produces a slope surface eruption. Eruption produces a preferential flow pathway that dominates water flow. Observed in FG quartz sand-rich and clay-sized quartz experiments. The surface erupts, suspends sediment in the water column (if smectite or clay-sized quartz is present), and forms conical deposit. In mixtures of 75 wt% clay-sized quartz, multiple eruptions and conical deposits formed. In mixtures of 0 wt% smectite and 75% clay-sized quartz, **B1** is the only observed failure behavior. **B2.** Sediment mixtures including cohesive sediments. Buildup of overpressure produces surface tension cracks, small subsurface cracks connected to the slope surface, and sand/clay boils. Surface cracks were observed in all smectite-containing mixtures. Sand/clay boils were observed in smectite mixtures ≥25 wt%. Flow is dominated by seepage flow. **C.** Further buildup of overpressure produces a subsurface fissure. Water flow is still dominated by seepage flow, with the subsurface fissure acting as a slope-internal flow pathway. **D.** The subsurface fissure developed in step **C** expands vertically and laterally, connecting with the slope surface and erupting. Smectite is suspended in the water column. Excess head continued to build until the eruption occurs, which produces a preferential flow pathway and reduces overpressure. **E.** Due to the reduction in built overpressure caused by the surface eruption in step **D**, the existing subsurface fissure reduces in lateral and vertical extent, collapsing and ending the surface eruption. The eruption from step D produces two deposits: a deposit immediately adjacent to the point of eruption and a distal, clay-enriched deposit resulting from the suspension of clay particles in the water column. **F.** The collapse of the existing subsurface fissure and preferential flow pathway in step E causes the buildup of overpressure. This buildup produces new subsurface fissures, some of which expand vertically and laterally and connect to the surface, creating new eruptions. This process mimics the process described for steps **C** – **E**. **G.** Eruptions in step **F** reduce overpressure but are inadequate to increase system permeability to levels sufficient to prevent further buildup of overpressure. This built overpressure causes subsurface fissures to expand and connect, separating sections of sediment from the parent slope. Eruptions in step **F** create deposits via the same processes as described in step **E**. The addition of several eruptions and rafting of sediment blocks produces preferential pathways which reduce overpressure and increase system permeability to levels high enough to prevent any further buildup of overpressure.

magnitude greater than cohesive forces (Mienert et al., 2010; Andresen and Huuse, 2011; Gay et al., 2011; Sun et al., 2012).

From our experimental observations and comparison with natural systems, we interpret that cohesive clays and overpressure are needed for formation of subsurface fissures in shallow sediments. It is, however, unclear if the rate of overpressure generation is a deciding factor in the formation of these features. Sediment loading and dehydration reactions in nature produce pressure at a slower rate than in our experiments. Other forces, such as ground accelerations, could produce overpressure rapidly, potentially at rates similar to those used in our experiments (Osborne and Swarbrick, 1997a; Kvalstad et al., 2005; Solheim et al., 2005; Hustoft et al., 2009; Dugan and Sheahan, 2012). Since subsurface fissures have been observed in nature (Mienert et al., 2010; Andresen and Huuse, 2011; Gay et al., 2011; Sun et al., 2012) and our physical experiments, the importance of the rate of overpressure generation requires more investigation.

Separation of sediment blocks (rafting) was observed in mixtures with 25, 75, and 90 wt% smectite. We attributed rafting to: (1) cohesion strong enough to maintain intact blocks; (2) permeabilities low enough to require alleviation of overpressure via a mechanism other than seepage flow; and (3) a rate of increase in overpressure (1–1.5 cm head/5 min) quick enough to form preferential flow pathways to reduce overpressure. The fast formation of these pathways reduced overpressure, channelizing flow to the water column and away from the blocks. None of the rafted blocks were remobilized rapidly downslope, and in only one case did a rafted block creep downslope. This result indicates overpressure can generate large-scale failure blocks, but additional drivers are likely needed to mobilize these blocks down slope at velocities necessary for tsunamigenesis. Our observed formation of subsurface fissures and isolated rafted sediment blocks may be analogous to the formation of weak layers in the natural environment (Elverhøi et al., 2010). Natural perturbations such as seismic shaking, currents, or internal waves may provide a driving force to mobilize rafted blocks in natural settings such as those observed along the Cascadia margin or the North Sea (Kvalstad et al., 2005; Scholz et al., 2016).

The absence of rafting in 50 wt% smectite-sand mixtures may indicate a balance created by fluid flow through subsurface fissures and connected pores. Since rafting was observed in 25 wt% smectite experiments, system cohesion should have been sufficient for rafting in systems with 50 wt% smectite. The permeability of mixtures with 50 wt % smectite was less than mixtures with 25 wt% smectite and greater than mixtures with >75 wt% smectite mixtures. While permeability of mixtures with 50 wt% smectite experiments was low, the development of subsurface fissure blowouts create higher permeability conduits preventing ovepressure from reach levels sufficient for lifting and separation of entire sediment blocks. Further analyses may be able to illuminate the causes of the lack of rafting at 50 wt% smectite but is beyond the scope of this study.

It is worth noting that despite the scale of our experiments and the similarity of magnitude between cohesive forces and overpressure in the flume, similar failure features have been connected to clay content in larger flume experiments (Elverhøi et al., 2010; Sawyer et al., 2012). Brittle deformation features such as surface cracking and hydraulic chimneys/subsurface fissures created in our experiments have also been observed in natural, clay-rich sediments (Hustoft et al., 2009; Mienert et al., 2010). We therefore interpret that our results – at the simplest level – reflect changes in failure behavior resulting from cohesive forces and permeabilities, rather experiment scaling.

6. Conclusions

To better understand submarine slope failure criteria and evolution, we used benchtop flume experiments and an infinite slope analysis to explore the impacts of permeability and cohesion on slope failures induced by overpressure. We investigated failures for different mixtures of fine-grained quartz sand homogeneously mixed with cohesive smectite clay or non-cohesive clay-sized quartz that were formed into a geometry similar to a prograding marine delta. Based on our experiments, we conclude:

- In high-permeability, sand-rich systems (0–5 wt% smectite), normalized overpressure required to induce failure was directly related to smectite content ($R^2 = 0.91$) and only a single failure event occurred, even with sustained or increased overpressure.
- In systems with smectite concentrations ≥ 25 wt%, normalized overpressure required to induce slope failure remained relatively constant at $\lambda^* = 1.52 \pm 0.55$ and a series of slope failures occurred with sustained or increased overpressure.
- Lower permeability systems have the potential for larger and repeated failures.
- Cohesion is necessary in producing brittle failure features (e.g., surface and subsurface fractures, rafted blocks).
- Overpressure can precondition a slope for tsunamigenic failure by producing rafted sediment blocks in sediment mixtures with 25–90 wt% smectite.

- Overpressure alone does not mobilize sediment blocks and thus is not likely to induce tsunamigenic slope failure.

Our results provide some baseline information on sediment behavior patterns that can help assess risk potential in different geological settings. Our experiments reveal that in coastal regions with supply of cohesive clays ≥25 wt%, shallow over-pressured sediments can produce slope failures capable of damaging seafloor infrastructure (via tension cracking or surface eruptions). Overpressure within shallow sediments with 25–90 wt% concentrations of cohesive clays can precondition slopes for tsunamigenic failure via the formation of subsurface fissures/piping and rafted blocks. These blocks, if rapidly mobilized, have the potential to generate. The incorporation of these risk criteria (clay-rich, over-pressured) into social vulnerability and hazard models could improve model accuracy by identifying areas preconditioned for submarine slope failure, areas previously considered low-risk or at-no-risk of tsunamigenesis during seismic activity (e.g., passive margins) and improve the accuracy of tsunami size forecasting/modelling.

Declaration of Competing Interest

The authors in this paper declare no conflicts of interests.

Data availability

Digital copies of data can be found at the Colorado School of Mines Data Repository under Hydrologic Science and Engineering Datasets.

Acknowledgments

This work was funded by NSF-OCE-1753680 and the Colorado School of Mines. This research benefited from discussions with D. Sawyer.

Appendix A. Supplementary data

Supplementary data to this article can be found online at https://doi.org/10.1016/j.margeo.2023.107079.

References

Andresen, K.J., Huuse, M., 2011. "Bulls-eye" pockmarks and polygonal faulting in the lower congo basin: relative timing and implications for fluid expulsion during shallow burial. Mar. Geol. 279, 111–127. https://doi.org/10.1016/j.margeo.2010.10.016.

Bardet, J.-P., Synolakis, C.E., Davies, H.L., Imamura, F., Okal, E.A., 2003. In: Bardet, J.-P., Imamura, F., Synolakis, C.E., Okal, E.A., Davies, H.L. (Eds.), Landslide Tsunamis: Recent Findings and Research Directions. Basel, Birkhäuser Basel, p. 426. https://doi.org/10.1007/978-3-0348-7995-8.

Beakawi Al-Hashemi, H.M., Baghabra Al-Amoudi, O.S., 2018. A review on the angle of repose of granular materials. Powder Technol. 330, 397–417. https://doi.org/10.1016/j.powtec.2018.02.003.

Bekins, B.A., McCaffrey, A.M., Dreiss, S.J., 1995. Episodic and constant flow models for the origin of low-chloride waters in a modern accretionary complex. Water Resour. Res. 31, 3205–3215.

Biscontin, G., Pestana, J.M., 2006. Factors affecting seismic response of submarine slopes. Nat. Hazards Earth Syst. Sci. 6, 97–107. https://doi.org/10.5194/nhess-6-97-2006.

Biscontin, G., Pestana, J.M., Nadim, F., 2004. Seismic triggering of submarine slides in soft cohesive soil deposits. Mar. Geol. 203, 341–354. https://doi.org/10.1016/S0025-3227(03)00314-1.

Bondevik, S., Løvholt, F., Harbitz, C., Mangerud, J., Dawson, A., Svendsen, J.I., 2005. The Storegga Slide tsunami - comparing field observations with numerical simulations. Mar. Pet. Geol. https://doi.org/10.1016/j.marpetgeo.2004.10.003.

Clare, M., et al., 2019. A Consistent global approach for the morphometric characterization of subaqueous landslides. Geol. Soc. Lond., Spec. Publ. 477, 455–477. https://doi.org/10.1144/SP477.15.

Dugan, B., Flemings, P.B., 2000. Overpressure and fluid flow in the New Jersey continental slope: implications for slope failure and cold seeps. Science 289, 288–291. https://doi.org/10.1126/science.289.5477.288.

Dugan, B., Sheahan, T.C., 2012. Offshore sediment overpressures of passive margins: mechanisms, measurement, and models. Rev. Geophys. 50, 1–20. https://doi.org/10.1029/2011RG000379.

Elger, J., Berndt, C., Rüpke, L., Krastel, S., Gross, F., Geissler, W.H., 2018. Submarine slope failures due to pipe structure formation. Nat. Commun. 9, 715. https://doi.org/10.1038/s41467-018-03176-1.

Elverhøi, A., Harbitz, C., Dimikis, P., Mohrig, D., Marl, J., Parker, G., 2000. On the dynamics of subaqueous debris flows. Oceanography 13, 109–117. https://doi.org/10.5670/oceanog.2000.20.

Elverhøi, A., de Blasio, F.V., Butt, F.A., Issler, D., Harbitz, C., Engvik, L., Solheim, A., Marr, J., 2002. Submarine mass-wasting on glacially-influenced continental slopes: processes and dynamics. Geol. Soc. Lond., Spec. Publ. 203, 73–87. https://doi.org/10.1144/GSL.SP.2002.203.01.05.

Elverhøi, A., Breien, H., de Blasio, F.V., Harbitz, C.B., Pagliardi, M., 2010. Submarine landslides and the importance of the initial sediment composition for run-out length and final deposit. Ocean Dyn. 60, 1027–1046. https://doi.org/10.1007/s10236-010-0317-z.

Elverhoi, A., Breien, H., De Blasio, F.V., Harbitz, C.B., Pagliardi, M., 2010. Submarine landslides and the importance of the initial sediment composition for run-out length and final deposit. Ocean Dyn. 60, 1027–1046. https://doi.org/10.1007/s10236-010-0317-z.

Fine, I.V., Rabinovich, A.B., Bornhold, B.D., Thomson, R.E., Kulikov, E.A., 2005. The grand banks landslide-generated tsunami of November 18, 1929: preliminary analysis and numerical modeling. Mar. Geol. 215, 45–57. https://doi.org/10.1016/j.margeo.2004.11.007.

Finn, W.D.L., 2003. Landslide-generated tsunamis: geotechnical considerations. In: Bardet, J.-P., Imamura, F., Synolakis, C.E., Okal, E.A., Davies, H.L. (Eds.), Landslide Tsunamis: Recent Findings and Research Directions. Basel, Birkhäuser Basel, pp. 1879–1894. https://doi.org/10.1007/978-3-0348-7995-8_6.

Forsberg, C.F., Locat, J., 2005. Mineralogical and microstructural development of the sediments on the mid-norwegian margin. In: Ormen Lange–an Integrated Study for Safe Field Development in the Storegga Submarine Area. Elsevier, pp. 109–122. https://doi.org/10.1016/B978-0-08-044694-3.50013-5.

Gamboa, D., Alves, T., Cartwright, J., 2011. Distribution and characterization of failed (mega)blocks along salt ridges, Southeast Brazil: Implications for vertical fluid flow on continental margins. J. Geophys. Res. Solid Earth 116. https://doi.org/10.1029/2011JB008357.

Garces, L.R., et al., 2010. Rapid Assessment of Community Needs and Fisheries Status in Tsunami-Affected Communities in Aceh Province, v. 53. Ocean & Coastal Management, Indonesia, pp. 69–79. https://doi.org/10.1016/j.ocecoaman.2009.12.004.

Gay, A., et al., 2011. Geophysical and geochemical evidence of large scale fluid flow within shallow sediments in the Eastern Gulf of Mexico, Offshore Louisiana. Geofluids 11, 34–47. https://doi.org/10.1111/j.1468-8123.2010.00304.x.

Gazioğlu, C., Yücel, Z.Y., Doğan, E., 2005. Morphological features of major submarine landslides of marmara sea using multibeam data. J. Coast. Res. https://doi.org/10.2112/03-0060.1.

Gee, M.J.R., Gawthorpe, R.L., Friedmann, S.J., 2006. Triggering and evolution of a giant submarine landslide, offshore Angola, revealed by 3D seismic stratigraphy and geomorphology. J. Sediment. Res. 76, 9–19. https://doi.org/10.2110/jsr.2006.02.

Gue, C.S., Soga, K., Bolton, M., Thusyanthan, N.I., 2010. Centrifuge Modelling of Submarine Landslide Flows: Conference on Physical Modelling in Geotechnics.

Haflidason, H., Sejrup, H.P., Nygård, A., Mienert, J., Bryn, P., Lien, R., Forsberg, C.F., Berg, K., Masson, D., 2004. The storegga slide: architecture, geometry and slide development. Mar. Geol. 213, 201–234. https://doi.org/10.1016/j.margeo.2004.10.007.

Hampton, M.A., Lee, H.J., Locat, J., 1996. Submarine landslides. Rev. Geophys. 34, 33–59. https://doi.org/10.1029/95RG03287.

Harbitz, C.B., Pedersen, G., Gjevik, B., 1993. Numerical simulations of large water waves due to landslides. J. Hydraul. Eng. 119, 1325–1342. https://doi.org/10.1061/(ASCE)0733-9429(1993)119:12(1325).

Harbitz, C.B., Løvholt, F., Bungum, H., 2014. Submarine landslide tsunamis: how extreme and how likely? Nat. Hazards 72, 1341–1374. https://doi.org/10.1007/s11069-013-0681-3.

Hornbach, M.J., Lavier, L.L., Ruppel, C.D., 2007. Triggering mechanism and tsunamogenic potential of the cape fear slide complex, U.S. Atlantic Margin. Geochem. Geophys. Geosyst. 8 https://doi.org/10.1029/2007GC001722 p. n/a-n/a.

Hustoft, S., Dugan, B., Mienert, J., 2009. Effects of rapid sedimentation on developing the nyegga pockmark field: constraints from hydrological modeling and 3-D seismic data, offshore mid-Norway. Geochem. Geophys. Geosyst. 10 https://doi.org/10.1029/2009GC002409 p. n/a-n/a.

Kaminski, P., Urlaub, M., Grabe, J., Berndt, C., 2020. Geomechanical behaviour of gassy soils and implications for submarine slope stability: a literature analysis. Geol. Soc. Lond., Spec. Publ. 500, 277–288. https://doi.org/10.1144/SP500-2019-149.

Kawakita, S., Asahina, D., Takemura, T., Hosono, H., Kitajima, K., 2020. Effect of hydraulic and mechanical characteristics of sediment layers on water film formation in submarine landslides. Prog. Earth Planet. Sci. 7 https://doi.org/10.1186/s40645-020-00375-7.

Kvalstad, T.J., Andresen, L., Forsberg, C.F., Berg, K., Bryn, P., Wangen, M., 2005. The storegga slide: evaluation of triggering sources and slide mechanics. Mar. Pet. Geol. 22, 245–256. https://doi.org/10.1016/j.marpetgeo.2004.10.019.

Lemke, R.W., 1967. Effects of the Earthquake of March 27, 1964 at Seward, v. 542-E. Geological Survey Professional Paper, Alaska, p. 53.

Liu, T., Lu, Y., Zhou, L., Yang, X., Guo, L., 2019. Experiment and analysis of submarine landslide model caused by elevated pore pressure. J. Marine Sci. Eng. 7 https://doi.org/10.3390/jmse7050146.

Locat, J., Lee, H., ten Brink, U.S., Twichell, D., Geist, E., Sansoucy, M., 2009. Geomorphology, stability and mobility of the currituck slide. Mar. Geol. 264, 28–40. https://doi.org/10.1016/j.margeo.2008.12.005.

Locat, J., ten Brink, U.S., Chaytor, J.D., 2010. The Block Composite Submarine Landslide, Southern New England Slope, U.S.A.: A Morphological Analysis. In: Submarine Mass Movements and Their Consequences, Dordrecht, Springer Netherlands, pp. 267–277. https://doi.org/10.1007/978-90-481-3071-9_22.

Løseth, H., Gading, M., Wensaas, L., 2009. Hydrocarbon leakage interpreted on seismic data. Mar. Pet. Geol. 26, 1304–1319. https://doi.org/10.1016/j.marpetgeo.2008.09.008.

Løvholt, F., Schulten, I., Mosher, D., Harbitz, C., Krastel, S., 2019. Modelling the 1929 grand banks slump and landslide tsunami. Geol. Soc. Lond., Spec. Publ. 477, 315–331. https://doi.org/10.1144/SP477.28.

Lynett, P., Liu, P.L.-F., 2003. Submarine landslide generated waves modeled using depth-integrated equations. In: Submarine Landslides and Tsunamis. Springer Netherlands, Dordrecht, pp. 51–58. https://doi.org/10.1007/978-94-010-0205-9_7.

Manton, B., Planke, S., Millett, J., Zastrozhnov, D., Mazzini, A., Muller, P., Myklebust, R., 2019. Hydrothermal vent complexes acting as preferential fluid migration pathways in the Møre and Vøring Basins. Geophys. Res. Abstr. v, 21.

Masson, D.G., Arzola, R.G., Wynn, R.B., Hunt, J.E., Weaver, P.P.E., 2011. Seismic triggering of landslides and turbidity currents offshore Portugal. Geochem. Geophys. Geosyst. 12 https://doi.org/10.1029/2011GC003839.

Mazzini, A., Svensen, H., Akhmanov, G.G., Aloisi, G., Planke, S., Malthe-Sørenssen, A., Istadi, B., 2007. Triggering and dynamic evolution of the LUSI Mud Volcano, Indonesia. Earth Planet. Sci. Lett. 261, 375–388. https://doi.org/10.1016/j.epsl.2007.07.001.

McAdoo, B.G., Pratson, L.F., Orange, D.L., 2000. Submarine landslide geomorphology, US Continental Slope. Mar. Geol. 169, 103–136. https://doi.org/10.1016/S0025-3227(00)00050-5.

McAdoo, B.G., Capone, M.K., Minder, J., 2004. Seafloor geomorphology of convergent margins: Implications for Cascadia seismic hazard. Tectonics 23, 1–15. https://doi.org/10.1029/2003TC001570.

Mienert, J., Vanneste, M., Haflidason, H., Bünz, S., 2010. Norwegian margin outer shelf cracking: a consequence of climate-induced gas hydrate dissociation? Int. J. Earth Sci. 99, 207–225. https://doi.org/10.1007/s00531-010-0536-z.

Mohrig, D., Marr, J.G., 2003. Constraining the efficiency of turbidity current generation from submarine debris flows and slides using laboratory experiments. Mar. Pet. Geol. 20, 883–899. https://doi.org/10.1016/j.marpetgeo.2003.03.002.

Mohrig, D., Elverhøi, A., Parker, G., 1999. Experiments on the relative mobility of muddy subaqueous and subaerial debris flows, and their capacity to remobilize antecedent deposits. Mar. Geol. 154, 117–129. https://doi.org/10.1016/S0025-3227(98)00107-8.

Mosher, D.C., 2009. International year of planet earth 7. oceans: submarine landslides and consequent tsunamis in Canada. Geosci. Can. 36, 179–190.

Odom, I.E., 1984. Smectite clay minerals: properties and uses. Philos. Trans. Royal Soc. London. Series A, Math. Phys. Sci. 311, 391–409. https://doi.org/10.1098/rsta.1984.0036.

Ohmachi, T., 2003. Tsunami simulation taking into account seismically induced dynamic seabed displacement, and acoustic effects of water. In: Submarine Landslides and Tsunamis. Springer Netherlands, Dordrecht, pp. 89–99. https://doi.org/10.1007/978-94-010-0205-9_10.

Osborne, M.J., Swarbrick, R.E., 1997a. Mechanisms for generating overpressure in sedimentary basins: a reevaluation. AAPG Bull. 81 (1997), 1023–1041 doi:10.1306/522B49C9-1727-11D7-8645000102C1865D.

Osborne, M.J., Swarbrick, R.E., 1997b. Mechanisms for generating overpressure in sedimentary basins: a reevaluation. AAPG Bull. 81, 1023–1041. https://doi.org/10.1306/522B49C9-1727-11D7-8645000102C1865D.

Prior, D.B., Coleman, J.M., Bornhold, B.D., 1982. Results of a known seafloor instability event. Geo-Mar. Lett. 2, 117–122. https://doi.org/10.1007/BF02462751.

Prior, D.B., Yang, Z.S., Bornhold, B.D., Keller, G.H., Lu, N.Z., Wiseman Jr., W.J., Wright, L.D., Zhang, J., 1986. Active Slope Failure, Sediment Collapse, and Silt Flows on the Modern Subaqueous Huanghe (Yellow River), v. 6. Geo-Marine Letters, Delta, pp. 85–95. https://doi.org/10.1007/BF02281644.

Sawyer, D.E., DeVore, J.R., 2015. Elevated shear strength of sediments on active margins: evidence for seismic strengthening. Geophys. Res. Lett. 42 https://doi.org/10.1002/2015GL066603.

Sawyer, D.E., Flemings, P.B., Buttles, J., Mohrig, D., 2012. Mudflow transport behavior and deposit morphology: role of shear stress to yield strength ratio in subaqueous experiments. Mar. Geol. v. 307–310, 28–39. https://doi.org/10.1016/j.margeo.2012.01.009.

Scholz, N.A., Riedel, M., Urlaub, M., Spence, G.D., Hyndman, R.D., 2016. Submarine landslides offshore vancouver island along the northern Cascadia Margin, British Columbia: why preconditioning is likely required to trigger slope failure. Geo-Mar. Lett. 36, 323–337. https://doi.org/10.1007/s00367-016-0452-8.

Schulten, I., Mosher, D.C., Piper, D.J.W., Krastel, S., 2019. A massive slump on the St. Pierre Slope, a new perspective on the 1929 grand banks submarine landslide. J. Geophys. Res. Solid Earth 124, 7538–7561. https://doi.org/10.1029/2018JB017066.

Silver, M.M.W., Dugan, B., 2020. The influence of clay content on submarine slope failure: insights from laboratory experiments and numerical models. Geol. Soc. Lond., Spec. Publ. 500, 301–309. https://doi.org/10.1144/SP500-2019-186.

Solheim, A., Bryn, P., Sejrup, H.P., Mienert, J., Berg, K., 2005. Ormen lange—an integrated study for the safe development of a deep-water gas Field within the storegga slide complex, NE Atlantic Continental margin; executive summary. Mar. Pet. Geol. 22, 1–9. https://doi.org/10.1016/j.marpetgeo.2004.10.001.

Steurer, J.F., Underwood, M.B., 2003. Clay mineralogy of mudstones from the nankai trough reference sites 1173 and 1177 and frontal accretionary prism site 1174. In: Proceedings of the Ocean Drilling Program, 190/196 Scientific Results, Ocean Drilling Program. https://doi.org/10.2973/odp.proc.sr.190196.211.2003.

Stigall, J., Dugan, B., 2010. Overpressure and earthquake initiated slope failure in the Ursa Region, Northern Gulf of Mexico. J. Geophys. Res. 115, B04101. https://doi.org/10.1029/2009JB006848.

Strasser, M., Stegmann, S., Bussmann, F., Anselmetti, F.S., Rick, B., Kopf, A., 2007. Quantifying subaqueous slope stability during seismic shaking: Lake Lucerne as model for ocean margins. Mar. Geol. 240, 77–97. https://doi.org/10.1016/j.margeo.2007.02.016.

Strout, J.M., Tjelta, T.I., 2005. In situ pore pressures: what is their significance and how can they be reliably measured? Mar. Pet. Geol. 22, 275–285. https://doi.org/10.1016/j.marpetgeo.2004.10.024.

Sun, Q., Wu, S., Cartwright, J., Dong, D., 2012. Shallow gas and focused fluid flow systems in the Pearl River Mouth Basin, Northern South China Sea. Mar. Geol. 315–318, 1–14. https://doi.org/10.1016/j.margeo.2012.05.003.

Tappin, D.R., Watts, P., McMurtry, G.M., Lafoy, Y., Matsumoto, T., 2001. The Sissano, Papua New Guinea Tsunami of July 1998 — Offshore evidence on the Source Mechanism. Mar. Geol. 175, 1–23. https://doi.org/10.1016/S0025-3227(01)00131-1.

Tappin, D.R., Watts, P., Grilli, S.T., 2008. The Papua New Guinea Tsunami of 17 July 1998: anatomy of a catastrophic event. Nat. Hazards Earth Syst. Sci. 8, 243–266. https://doi.org/10.5194/nhess-8-243-2008.

Tappin, D.R., Grilli, S.T., Harris, J.C., Geller, R.J., Masterlark, T., Kirby, J.T., Shi, F., Ma, G., Thingbaijam, K.K.S., Mai, P.M., 2014. Did a submarine landslide contribute to the 2011 Tohoku Tsunami? Mar. Geol. 357, 344–361. https://doi.org/10.1016/j.margeo.2014.09.043.

ten Brink, U.S., Lee, H.J., Geist, E.L., Twichell, D., 2009. Assessment of tsunami hazard to the U.S. East Coast using relationships between submarine landslides and earthquakes. Mar. Geol. 264, 65–73. https://doi.org/10.1016/j.margeo.2008.05.011.

ten Brink, U.S., Chaytor, J.D., Geist, E.L., Brothers, D.S., Andrews, B.D., 2014. Assessment of Tsunami Hazard to the U.S. Atlantic Margin. Marine Geol. 353, 31–54. https://doi.org/10.1016/j.margeo.2014.02.011.

ten Brink, U.S., Andrews, B.D., Miller, N.C., 2016. Seismicity and Sedimentation Rate Effects on Submarine Slope Stability. Geology 44, 563–566. https://doi.org/10.1130/G37866.1.

Terzaghi, K., 1956. Varieties of Submarine Slope failures: Eighth Texas conference on Soil Mechanics and Foundation Enginnering, pp. 1–21.

Terzaghi, K., Peck, R.B., Mesri, G., 1996. Soil Mechanics in Engineering Practice: New York. Wiley, Wiley-Interscience publication. https://books.google.com/books?id=bAwVvO71FXoC.

Tewfik, A., Andrew, N.L., Bene, C., Garces, L., 2008. Reconciling poverty alleviation with reduction in fisheries capacity: boat aid in Post-Tsunami Aceh, Indonesia. Fish. Manag. Ecol. 15, 147–158. https://doi.org/10.1111/j.1365-2400.2008.00597.x.

Underwood, M.B., Deng, X., 1997. Clay mineralogy and clay geochemistry in the vicinity of the Décollement Zone, Northern Barbados Ridge. In: Proceedings of the Ocean Drilling Program, 156 Scientific Results, Ocean Drilling Program. https://doi.org/10.2973/odp.proc.sr.156.001.1997.

Urlaub, M., Zervos, A., Talling, P.J., Masson, D.G., Clayton, C.I., 2012. How do ~2° slopes fail in areas of slow sedimentation? a sensitivity study on the influence of accumulation rate and permeability on submarine slope stability. In: Yamada, Y., Kawamura, K., Ikehara, K., Ogawa, Y., Urgeles, R., Mosher, D., Chaytor, J., Strasser, M. (Eds.), Submarine Mass Movements and their Consequences. Dordrecht, Springer, Netherlands, pp. 277–287.

Vanneste, M., Harbitz, C.B., De Blasio, F.V., Glimsdal, S., Mienert, J., Elverhøi, A., 2011. The Hinlopen–Yermak Landslide, Arctic Ocean - geomorphology, landslide dynamics, and tsunami simulations, *in* Mass-transport deposits in deepwater settings. SEPM (Society for Sedimentary Geology) 509–527. https://doi.org/10.2110/sepmsp.096.509.

Watts, P., 1997. Water Waves Generated by Underwater Landslides [Doctoral Thesis]:. California Institute of Technology, p. 334.

Williams, J.H., et al., 2022. Tsunami damage and post-event disruption assessment of road and electricity infrastructure: a collaborative multi-agency approach in ōtautahi Christchurch, Aotearoa New Zealand. Int. J. Disaster Risk Reduct. 72, 102841. https://doi.org/10.1016/j.ijdrr.2022.102841.

Zengaffinen, T., Løvholt, F., Pedersen, G.K., Harbitz, C.B., 2020. Effects of rotational submarine slump dynamics on tsunami genesis: New insight from idealized models and the 1929 grand banks event. In: Geological Society Special Publication, Geological Society of London, 500, pp. 41–61. https://doi.org/10.1144/SP500-2019-201.